



RF design and study of a 325 MHz 7 MeV APF IH-DTL for an injector of a proton medical accelerator

Xuan Li^{1,2,3} · Yue-Hu Pu^{1,2,3,4} · Fan Yang⁴ · Xiu-Cui Xie^{2,4} · Qiang Gu^{1,2,3} · Jian Qiao^{2,3} · Ming-Hua Zhao^{2,3}

Received: 28 January 2019/Revised: 28 April 2019/Accepted: 29 April 2019/Published online: 10 August 2019
© China Science Publishing & Media Ltd. (Science Press), Shanghai Institute of Applied Physics, the Chinese Academy of Sciences, Chinese Nuclear Society and Springer Nature Singapore Pte Ltd. 2019

Abstract A compact interdigital H-mode drift-tube linac (IH-DTL) with the alternating-phase-focusing (APF) method, working at 325 MHz was designed for an injector of a proton medical accelerator. When fed in with a proper RF (radio frequency) power, the DTL cavity could establish the corresponding electromagnetic field to accelerate the “proton bunches” from an input energy of 3 MeV to an output energy of 7 MeV successfully, without any additional radial focusing elements. The gap-voltage distribution which was obtained from the CST[®] Microwave Studio software simulations of the axial electric field was compared with that from the beam dynamics, and the errors met the requirements within $\pm 5\%$. In this paper, the RF design procedure and key results of the APF IH-DTL, which include the main RF characteristics of the cavity, frequency sensitivities of the tuners, and coupling factor of the RF power input coupler are presented.

Keywords Proton therapy · Proton medical accelerator · Injector · Drift-tube linac (DTL) · Interdigital H-mode (IH) · Alternating-phase-focusing (APF)

1 Introduction

Over the past few decades, various types of cancer have become a primary cause for human mortalities. Particularly, in current day China, on an average, seven patients are diagnosed with malignant tumors every minute [1]. With the rapid development of particle accelerator technologies and related medical treatment techniques, usage of energetic particle beams such as protons, heavy ions, and electrons supplied by these accelerators is considered to be one of the most efficient and practical ways to treat cancers. Particularly, proton accelerators are getting more and more attention nowadays due to the unique Bragg peak of proton beams, which helps to deliver a more effective treatment and a higher quality of life for the cancer patients.

The Advanced Proton Therapy Facility (APTRON) is a dedicated proton therapy facility located in the Ruijin hospital proton therapy center, Shanghai Jiaotong University School of Medicine. It is constructed by Shanghai APACTRON Particle Equipment Co. Ltd, which is a joint-stock company held by Shanghai Institute of Applied Physics (SINAP) and two other stakeholders. A schematic layout of APTRON is presented in Fig. 1. There are three treatment terminals—a fixed beam room, an eye treatment room, and a 180-degree rotating gantry room. The accelerator of the facility consists of a 7 MeV linear accelerator as the injector and a synchrotron accelerator with proton energy ranging from 70 MeV to 250 MeV. The

This work was supported by the National Key Research and Development Program of China (No. 2016YFC0105408).

✉ Yue-Hu Pu
puyuehu@sinap.ac.cn

- ¹ Shanghai Advanced Research Institute, Chinese Academy of Sciences, Shanghai 201210, China
- ² Shanghai Institute of Applied Physics, Chinese Academy of Sciences, Shanghai 201800, China
- ³ University of Chinese Academy of Sciences, Beijing 100049, China
- ⁴ Shanghai APACTRON Particle Equipment Co., Ltd, Shanghai 201800, China



Fig. 1 Overview of the APTRON facility

synchrotron has a circumference of 24.6 m and is composed of eight dipoles and twelve quadrupoles [2–4]. It is equipped with the resonant slow beam extraction method.

The 7 MeV injector is an important component of the APTRON facility and consists of a Duo-Plasma-IS, a low energy beam transport (LEBT) section, and two linacs arranged one after the other [5–8]. The first linac is a radio frequency quadrupole (RFQ) linac and the second is a conventional Alvarez-type drift-tube linac (DTL). As in a conventional DTL, a synchronous phase of nearly -30° is chosen to offer longitudinal focusing force as well as large acceptance. However, this negative phase array inevitably defocuses the beam transversely or radially. To overcome the defocusing force, a series of quadrupoles are employed to focus the beam transversely. There are two types of quadrupoles: electromagnets and permanent magnets; however, both of them make the conventional DTL heavy, bulky, and costly. Consequently, the development of a compact injector plays a key role in constructing a cost-effective proton therapy facility.

With a view to providing a compact injector to the facility, we proposed a scheme that replaces the conventional Alvarez-type DTL with a new DTL in the mass production phase. The new DTL adopts the interdigital H-mode (IH) structure working at 325 MHz to operate compatibly with the current RFQ. The alternating-phase-focusing (APF) method is employed for focusing the beam in the IH-DTL. The design work for the beam dynamics of this DTL has been already demonstrated [2]. Two more key aspects of the injector in the proposed scheme, namely the

RF design and the study of the APF IH-DTL cavity, are presented in this paper.

In the following sections, the principle and design procedure are presented first. This is followed by the design, simulation, and analysis of the main parameters which include the cavity, gap-voltage distribution, tuners, and the coupler. Finally, some concluding remarks on the design are provided.

2 Principle and procedure

2.1 Overview of the APF IH-DTL

Interdigital H-mode (IH) as an idea was first proposed in the 1950s by Blewett [9]. One of the key features of the IH structure is that its capacitive load is very high compared with a conventional DTL [10–12]. Consequently, for the same operating frequency, the IH structure has a smaller radius than a conventional DTL. This feature of the IH-DTL is an obvious advantage due to a significant reduction in the cavity size.

The alternating-phase-focusing (APF) DTL was also first proposed in the 1950s by Good [13]. In principle, an APF involves a sequence of negative and positive accelerating phases that appear alternately between groups of adjacent tubes. When the particles go through these different gaps and tubes along a longitudinal axis, the negative phase sections focus on the particle bunches longitudinally and defocus them radially. Conversely, the positive phase sections focus on the particle bunches

radially and defocus them longitudinally. After passing through several sinusoid-like periods in the sequence of alternating phases, the particles will be simultaneously focused, both longitudinally and radially. Figure 2 shows the principle behind the APF method. Both longitudinal and radial stability are achieved with just an RF accelerating field. Hence, there is no requirement of any additional focusing elements inside the drift tubes (DTs). This, in turn, leads to not only a reduction in the size of the DTs, but also savings in the cost of construction and maintenance of the whole cavity [14].

Unlike the Alvarez-type DTL, which excites the TM_{010} mode, the IH-DTL cavity excites the TE_{111} mode. Figure 3 shows the basic principle of the IH-DTL and its structure. It consists of a series of DTs, which are supported by stems connecting alternately to the opposite walls of the cavity.

2.2 Design procedure

The basic requirement of the RF design for the APF IH-DTL is getting the right voltage distribution between adjacent tubes along the longitudinal axis as required by the beam dynamics. As per the principle of the IH-DTL cavity, once a proper RF power is fed into the cavity, a longitudinal electric field is established directly in the structure shown in Fig. 3; however, it cannot accelerate the particles efficiently. Furthermore, there is no focusing element in the cavity to focus the protons, and the motion of protons inside the APF IH-DTL is only determined by the electromagnetic (EM) field distribution. As mentioned in [10], the EM field distribution would depend strongly on the whole structure of the cavity, including the radii of the cavity, the geometries of the ridge, the ridge tuner (RT) and the stems, the diameters of the DTs, RF power feed coupler, etc. Any geometrical changes of these components could lead to distribution variation of the EM field. Therefore, it is necessary to employ an efficient simulating procedure for designing the above components. In this study, we used CST[®] Microwave Studio (MWS) as the 3D EM solver to establish the model, carry out the simulations, and optimize the structure [14, 15].

A flowchart depicting the design procedure that we developed for the APF IH-DTL cavity is shown in Fig. 4.

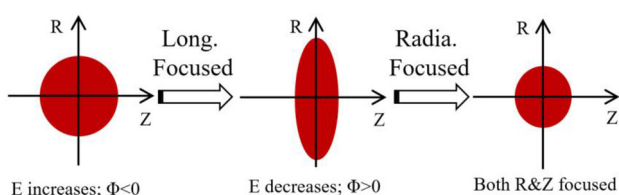


Fig. 2 Illustration of the principle of the APF. E is the accelerating electric field

3 Design and simulation

3.1 General parameters and considerations

Besides achieving the right gap-voltage distribution, another important objective of the RF design is to have a high shunt impedance, which leads to a low RF power dissipation on the cavity walls. Additionally, the cavity should operate stably under the high RF power condition, which requires the peak surface electric field E_s inside the cavity to be lower than a value described as a multiplication of the Kilpatrick limit E_K [13, 14, 16]. Following the aforementioned earlier studies, we have empirically taken E_s to be $\leq 1.6E_K$ in our APF cavity design. Then, a 3D model of the APF cavity is constructed, and the electromagnetic field and the cavity wall loss are analyzed by using the CST[®] MWS software.

3.2 Cavity design

According to Eq. (1), the frequency of the cavity is mainly determined by the inductance and the capacitance of the whole IH-DTL structure. The inductance mainly depends on the cross-sectional area enclosed by the cavity walls, the stems, the DTs, and the two ridges. Correspondingly, the capacitance mainly comes from the gaps between the DTs, gap between the two ridges, the stems, and the RF cavity walls [10].

$$f \propto \frac{1}{\sqrt{L_e C_e}}, \quad (1)$$

where f is the operating frequency, L_e and C_e are the effective inductance and capacitance, respectively. Because the velocity of protons at the exit of the cavity is 1.52 times that at the entrance of the cavity, it gives rise to an increase in the length of the DTs and the gaps among the DTs. This results in a maldistribution of the capacitance from the entrance to the exit. As a consequence, the E-field would peak near the entrance of the cavity and drop to zero near the exit of the cavity. Furthermore, the APF method introduces another kind of longitudinal distribution modulation of the DTs [17], which makes the situation further complicated.

In order to get the maximum accelerating efficiency, a balanced uniform longitudinal E-field distribution along the beam axis should be achieved. To achieve the same, we modified the inner radii of the cavity as a function of the distance from the cavity entrance. This modification of the cavity inner radii was performed incrementally, in a few steps, rather than in a continuous manner. Along the whole cavity length of 1514.6 mm, we divided the cavity into 15 sections longitudinally; each of the first fourteen sections is 100 mm in length; and the last section at the cavity exit

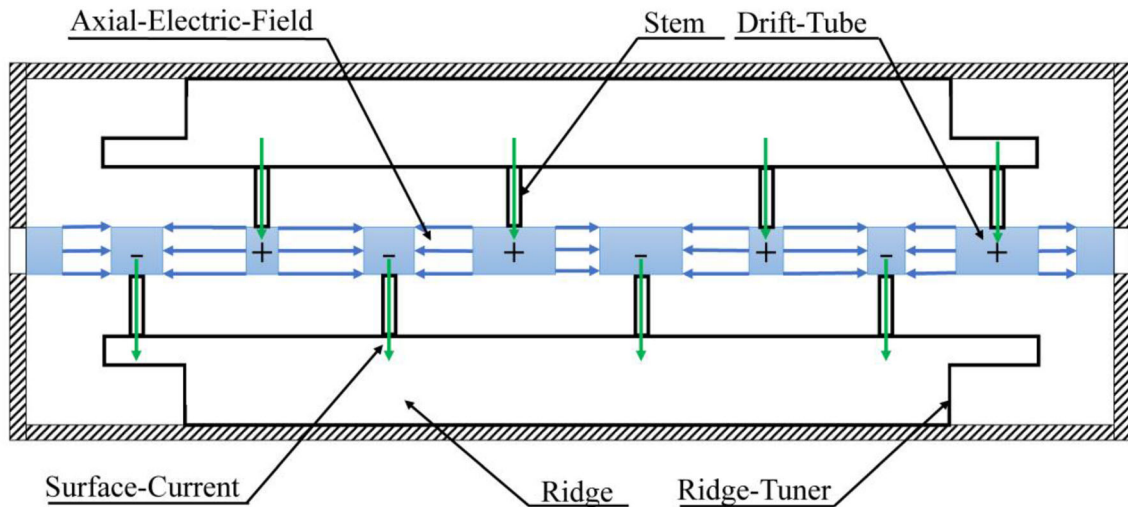


Fig. 3 Illustration of the principle of IH-DTL structure

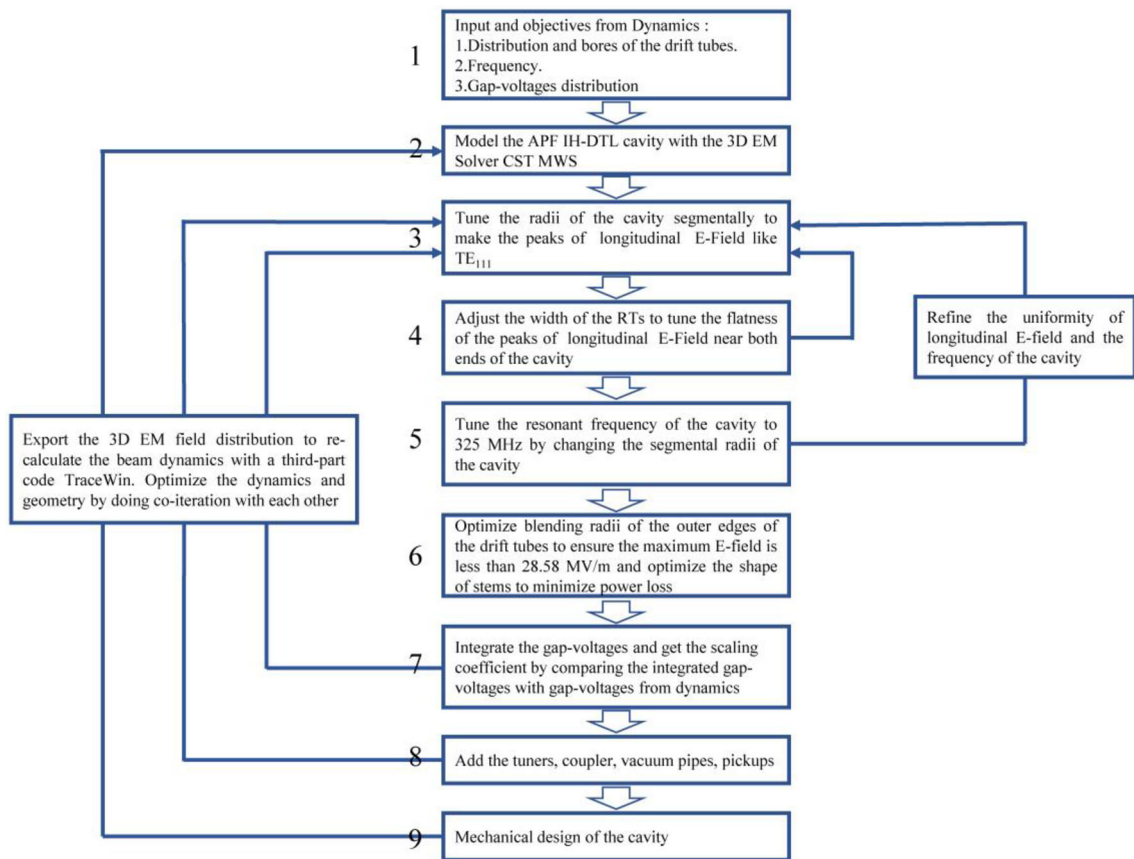


Fig. 4 Flowchart of the design procedure for the APF IH-DTL cavity

neighborhood is 114.6 mm long. After several iterative modifications and simulations of the radii of these 15 sections, we obtained the axial component of the electric field of the standard TE_{111} mode shape along the beam axis. The simulation results of the on-axis electric field obtained using CST[®] MWS are shown in Fig. 5. The

dotted red curve is the initial field strength distribution before the optimization, and the dashed blue curve corresponds to the results after adjustment of radii of the segments. The solid green curve is the on-axis electric field distribution after the optimization of the ridge shapes on both ends of the cavity. Further, flatness in the on-axis field

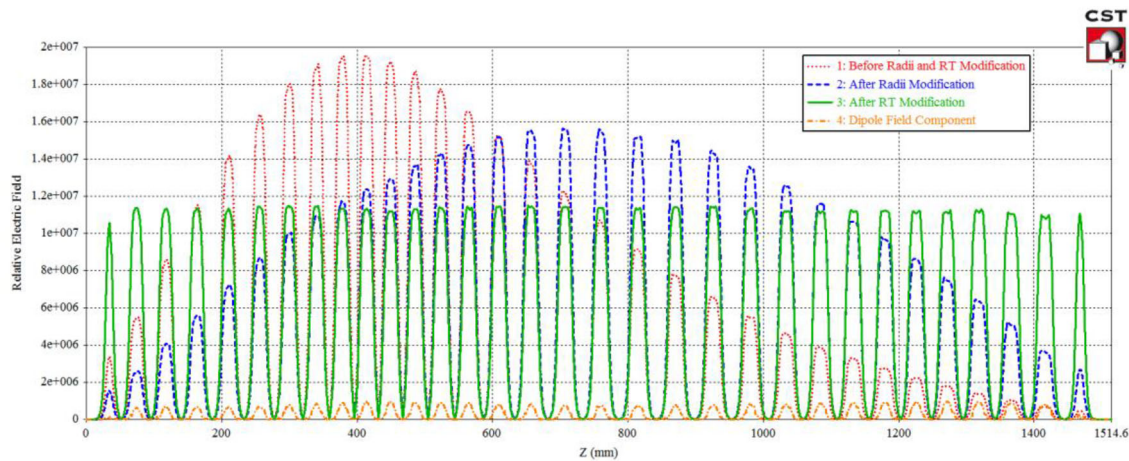


Fig. 5 (Color online) Axial component of the electric field along the center of the beam axis. The red (Dotted), blue (Dashed), and green (solid) curves show electric field distributions before radii and RT

modification, after radii modification, and after RT modification, respectively. The orange (Dash-dot) curve shows the dipole field component

distribution was obtained by adjusting the geometry of the ridge tuners (RT) or the ridge ends on the cavity, following the design procedure described in Fig. 4. Then, an ideal $TE_{11(0)}$ -like field distribution is achieved.

The next task is to tune the shape of the cavity to get the designed operating frequency of 325 MHz required from the beam dynamics [2]. Starting from the radii arrived at, in the previous step, we changed the radii of all the 15 segments simultaneously by a given amount, until we got the frequency of 325 MHz. This inevitably would influence the flatness of the axial component of the electric field along the beam axis. Hence, steps 3–5 were iteratively carried out to retain the flatness. The relation between the cavity resonant frequency and the cavity radii was analyzed during the optimization of the APF IH-DTL. Due to the irregular radii distribution longitudinally, we chose one of the fourteen radii to study the sensitivity of frequency, and the result is plotted in Fig. 6. According to Fig. 6, the corresponding sensitivity between frequency and radius is about -2.9 MHz/mm. If the required frequency accuracy is 100 kHz, the corresponding machining precision should be about 34 μ m.

Compared with a sensitivity of -0.8 MHz/mm [13] between the resonant frequency and the cavity radius variation of a conventional Alvarez-type DTL, it appears that the resonant frequency of the APF IH-DTL cavity is very high, the reason being that the IH-DTL has a relatively small cavity radius when compared with an Alvarez-type DTL. Nevertheless, the higher sensitivity implies higher accuracy and better stability requirement on the cooling system of the cavity.

The peak surface electric field E_s inside the cavity is another important constraint during the cavity design. In normal-conducting cavities like the IH-DTL, too high an E_s

could lead to an electrical breakdown or sparking while operating with high RF power. According to the Kilpatrick criterion [13, 18, 19], the relationship between the E_s and the cavity resonant frequency is expressed by the following two Eqs. (2) and (3):

$$f(\text{MHz}) = 1.64E_K^2 e^{-8.5/E_K}, \quad (2)$$

$$E_s = bE_K, \quad (3)$$

where f is the operating frequency (MHz), E_K is known as the Kilpatrick limit (MV/m), and b is known as the bravery factor. According to some previous studies [5, 14, 17] and based on the consideration of a conservative design of the first APF IH-DTL, the typical value of the bravery factor b of our cavity was considered to be no more than 1.6. In our design, the value of E_K was 17.86 MV/m. Substituting the values of b and E_K in Eq. (3), we obtained the E_s in the 325 MHz APF IH-DTL as 28.58 MV/m.

According to the electric field distribution inside the IH-DTL cavity shown in Fig. 7, E_s primarily occurs on the outer edge of the DTs near the exit of the cavity (a model of which is shown in Fig. 8a). Therefore, we should reduce the E_s at this location. This can be remedied by blending the outer edge of the DTs and optimizing the blending radii to get an appropriate value of the E_s . The relation between the bravery factor b and the blending radii is shown in Fig. 9. Although a blending radius of 2 mm could meet the requirement for b to be less than 1.6, to minimize the dissipation power on the surface of the walls, a blending radius of about 5 mm was considered a better choice. This corresponds to a b of 1.53. However, considering that some DTs have a very short length of 16.5 mm, and the upper radius of the stems was only about 4 mm, we determined that a blending radius of 4 mm would ensure consistency

Fig. 6 Relation between the resonant frequency and the radius variation. R^2 is the trend line reliability

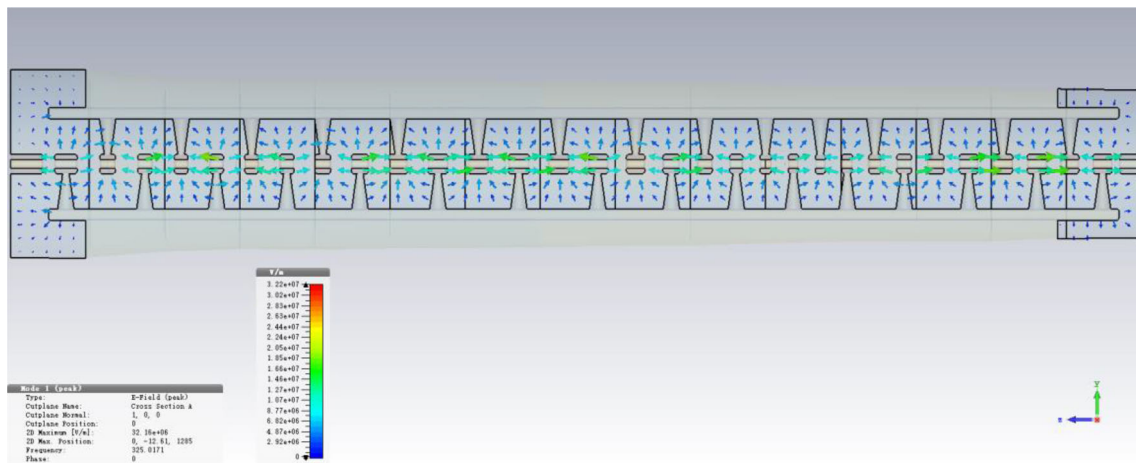
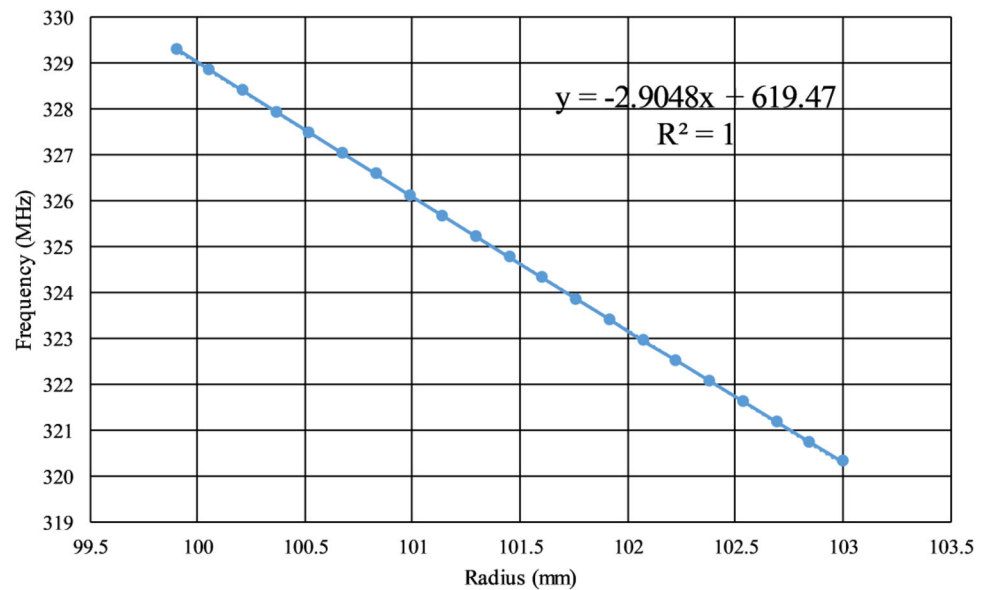


Fig. 7 (Color online) Electric field distribution inside the IH-DTL cavity by CST[®] MWS

among all the blending radii of the DTs. At this blending radius, the corresponding $E_s = 1.53E_K$.

To get a higher Q or a lower dissipation of power inside the cavity, two more main components needed to be optimized, namely the two ridges (upper and lower) and the stems (31 nos) [10, 14, 17]. The ridges used for the cavity were designed to have a rectangular cross section as shown in Fig. 10a. Narrower ridges have the advantage of reducing the capacitance between the upper and lower ridges and thus providing a better shunt impedance, as shown in Fig. 10b. However, the DTs, the stems, and ridges were to be machined from a massive block of copper, and hence, we had to consider the mechanical strength, the complexities of the manufacturing operations, and the space requirements for the cooling water channels inside the ridges; so the width of the ridges was set as 30 mm.

According to the field distribution of $TE_{11(0)}$ mode and the simulation results, the RF current is primarily concentrated upon the surface of the stems as shown in Fig. 11. Hence, to reduce the RF power dissipation, an effective solution would be to reduce the resistance distribution of the stems. In other words, thicker stems would be preferable. However, considering the ridge width, which was 30 mm, and the blending space for the edge connecting the stems and the ridges, both of which have the same blending radius of 2 mm, the maximum allowable radius of the lower end of the stems was 11 mm. In order to suppress the transverse dipole component of the electric field, we employed a cone-shaped stem as shown in Fig. 8c. The upper end of the stem, which is connected to the DT, is thinned to reduce the transverse component. Considering other design factors including the resistance, the length limit of the DTs, the mechanical strength, and

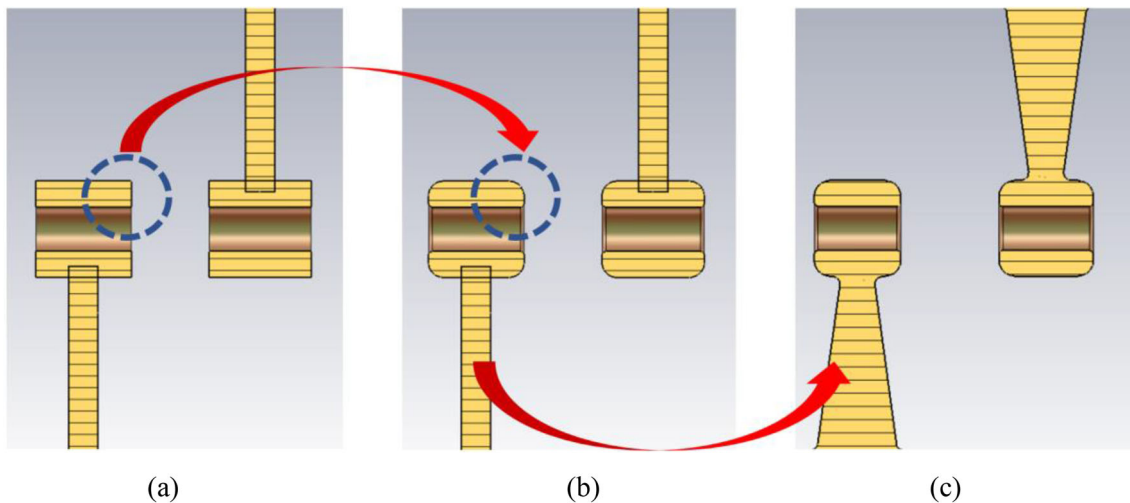


Fig. 8 Optimization of the outer edge of the DTs and the shape of the stems. From **a** to **b**, it shows the shape improvement of the outer edge of DTs from **b** to **c**, it shows the shape improvement of the stems. The final optimized DTs with stems are shown in **c**

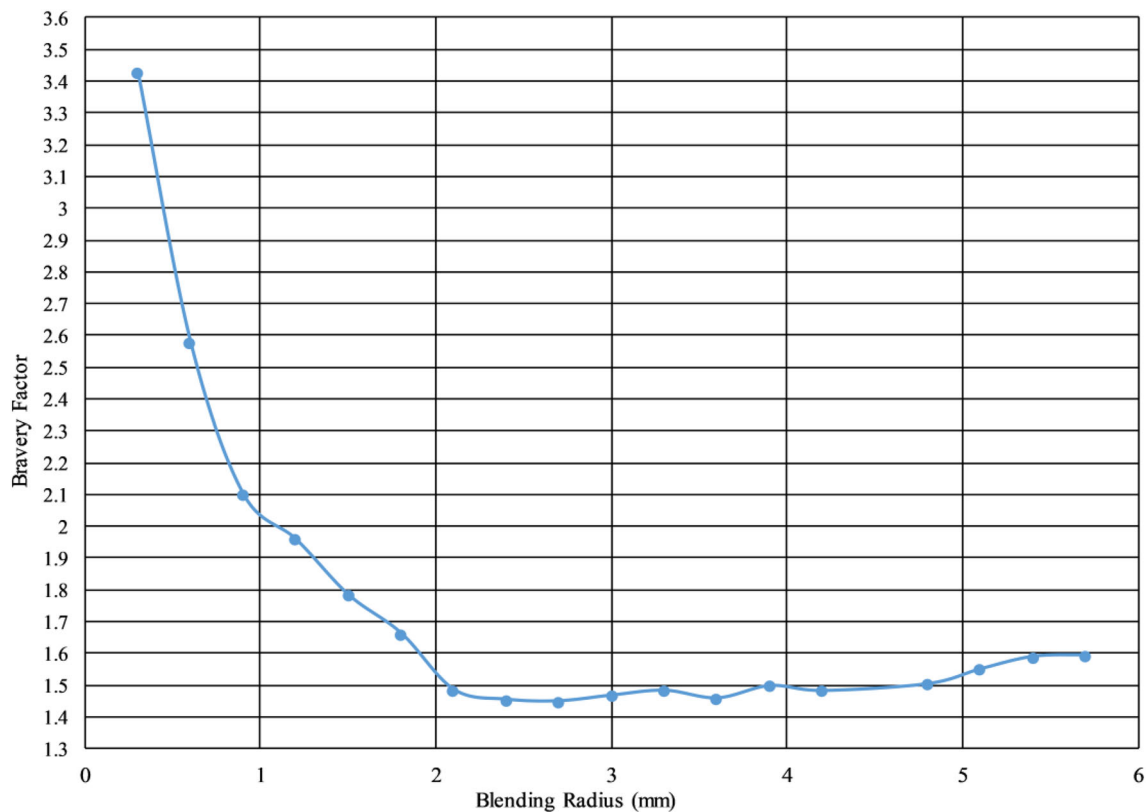


Fig. 9 Relation between the bravery factor and the blending radius on the outer edge of DTs

the blending space for the edge connecting the stems and the DTs, the upper radius of the stems was chosen to be 4 mm. The corresponding simulation results from CST[®] MWS indicated that the transverse dipole component of the electric field was less than 10% of the axial accelerating electric field (see Fig. 5); this meets the requirement as calculated from the beam dynamics [2].

After finalizing the design parameters as described above, we used the post-processing module of CST[®] MWS to get the gap-voltage distribution. Multiplying the gap-voltage distribution by a proper scaling coefficient, we notice that there is a good consistency between the voltage distributions from the CST[®] simulation and that from the beam dynamics (see Fig. 12). At this stage, the exported

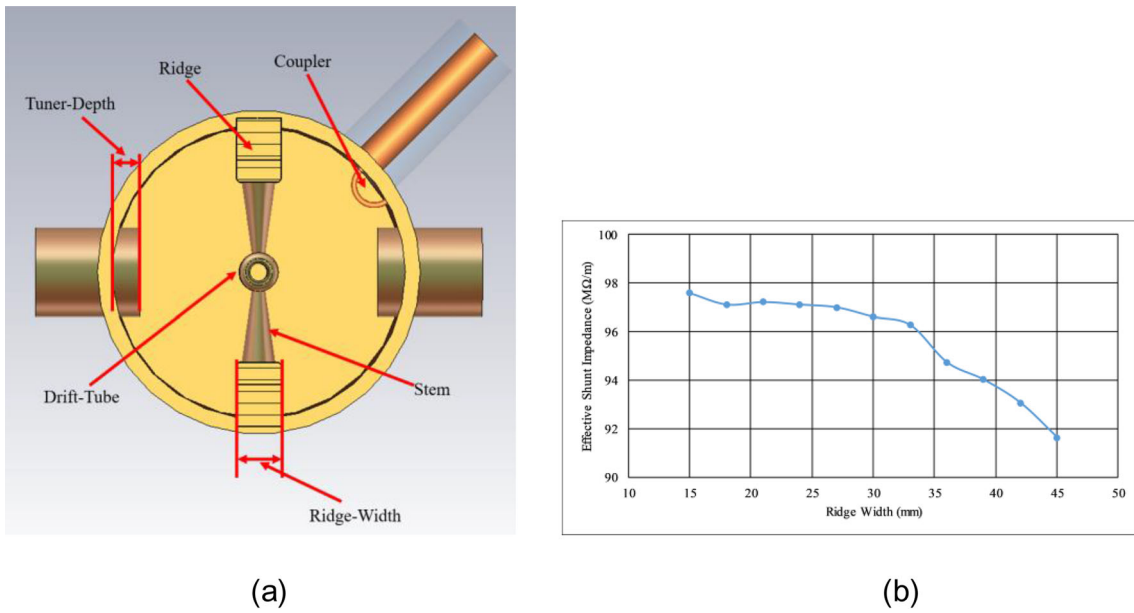


Fig. 10 Design considerations for the ridges. **a** Transverse cross section of the APF IH-DTL with the outer wall, **b** relation between the effective shunt impedance and the ridge width (**b**)

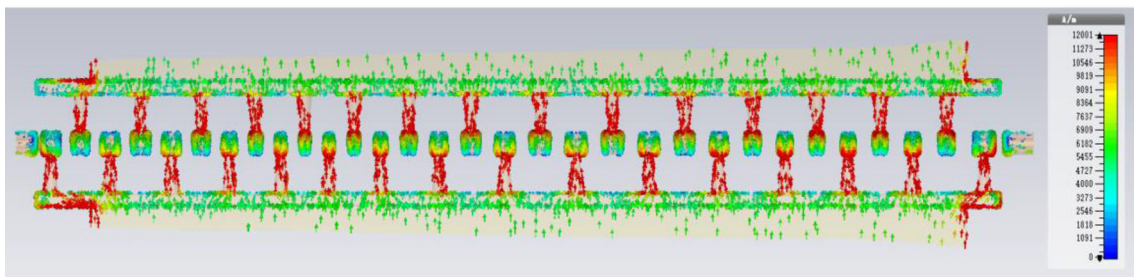
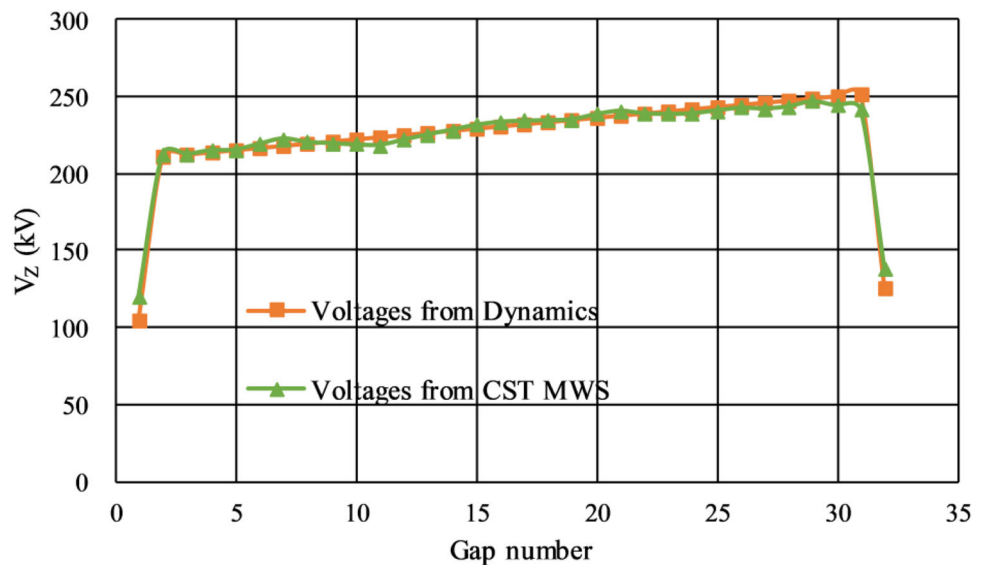


Fig. 11 (Color online) The RF current distribution inside the APF IH-DTL cavity. Red arrows on the surface of the cone-shaped stems indicate higher power loss density zones

Fig. 12 (Color online) Gap voltage along the beam axis as a function of the gap number after the co-iteration with the beam dynamics. Gap number is the number of the accelerating gaps. The orange (Squares) and the green (Triangle up) curves show the voltages required from dynamics and those calculated by CST[®] MWS, respectively



3D EM field and the scaling coefficient were provided to a third party code called “TraceWin” to recalculate the beam dynamics. In general, there will be some minor improvements in the dynamics and the cavity design. By iterating several times between the steps 3–7 (shown in Fig. 4), we obtained the optimized parameters for the dynamics and the cavity.

The errors in the voltages were calculated as $\Delta V/V_d = (V_C - V_d)/V_d$, where V_C is the voltage calculated by CST[®] MWS and V_d is the voltage required from the beam dynamics. The errors in the gap voltages of the 32 gaps are shown in Fig. 13a. It shows that an error of around $\pm 5\%$ was observed at the 1st, 31st, and 32nd gaps, while gap voltages for the left 29 gaps were optimized to the voltage required from the beam dynamics within an accuracy of $\pm 2\%$ and met the beam dynamics requirements [2].

The lengths of the DTs along the beam axis are also critical to the cavity design and are dependent on the precision of the computer numerical control (CNC) lathe and the machining process used for manufacturing the DTs. The precision of the start and end point positions of each DT during the machining determines the length of the DT. The errors in the lengths of the DTs result in a voltage variation. To meet the gap voltage errors requirement of $\pm 2\%$ from the beam dynamics, we analyzed the voltage variation on several error ranges of drift-tube lengths from 10 to 120 μm with an interval of 10 μm . In each case, the DTs with random errors were generated and evaluated. The results are shown in Fig. 13b. Allowing for a safe margin and the precision which the machining process could handle, the tolerance of the DTs was determined to be within $\pm 50 \mu\text{m}$, and this meets the gap voltage error of $\pm 2\%$ from the beam dynamics [2].

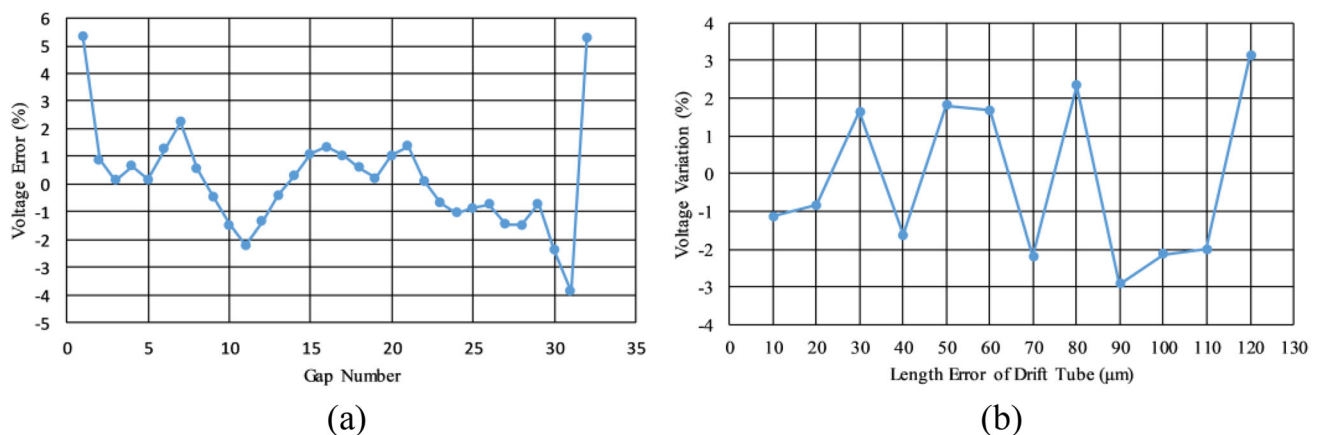


Fig. 13 Error analyses **a** errors of gap voltage, $\Delta V/V_d = (V_C - V_d)/V_d$, as functions of the gap numbers after the co-iteration with the beam dynamics; **b** gap-voltage variation caused by length error of the DT

3.3 Tuners design

Once the cavity was constructed, it would be impossible to fine tune the electric field distribution along the beam axis and the operating frequency of the cavity, as it would require changing the cavity’s radii. Based on an understanding of the perturbation theorem and the coupling of cavity EM field modes, eight inductive cylindrical copper tuners were installed on the horizontal plane of the cavity to fine tune the electric field distribution and tune the frequency [20]. These tuners were inserted into the cavity, alternately on the left and right sides, and were spaced apart longitudinally with an interval of approximately 108 mm. Figure 14 shows a schematic of their arrangement in the cavity. Furthermore, Fig. 15 depicts the relation between the frequency change of the cavity and the tuner depth (See Fig. 10a for tuner depth) for different tuner diameters. Considering the space available for tuner installation and the frequency tuning accuracy or ability of the tuners, the diameter of the tuners for our installation was determined to be 60 mm. The eight tuners have a total frequency adjusting ability of 136 kHz/mm. Thus, each tuner has an adjusting ability of 17 kHz/mm, and this is considered sufficient to tune the cavity frequency.

3.4 Coupler design

Based on the characteristics of the $TE_{11(0)}$ mode and the EM field distribution inside the cavity, the method of magnetic coupling is adopted to feed the high RF power into the APF IH-DTL cavity. According to the previous calculation by CST[®] MWS, the maximum RF power dissipation on the wall is about 156 kW, but the actual power dissipation P_c of cavity is 195 kW by factoring in a safety factor of 1.25 for the safe operation of the cavity. The pulse peak beam power P_b is given by $P_b = I_b \times U_b$, where, I_b is

Fig. 14 (Color online) 3D model of the APF IH-DTL in CST[®] MWS. The outer cylindrical wall is removed; cavity inner volume of the latter part is shown in light blue

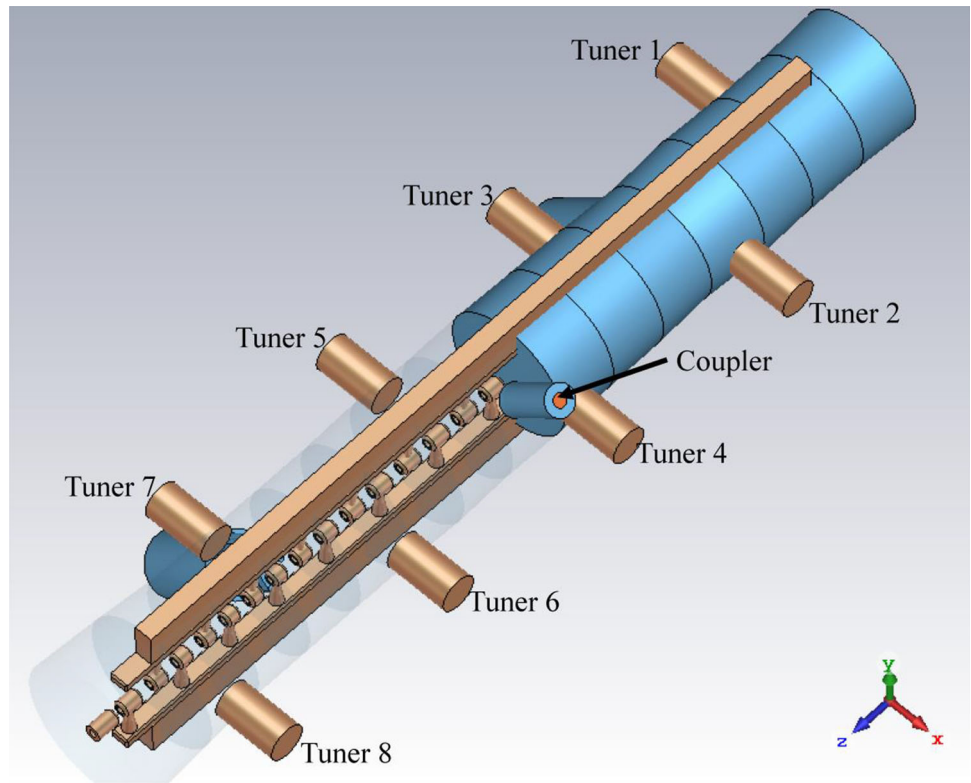
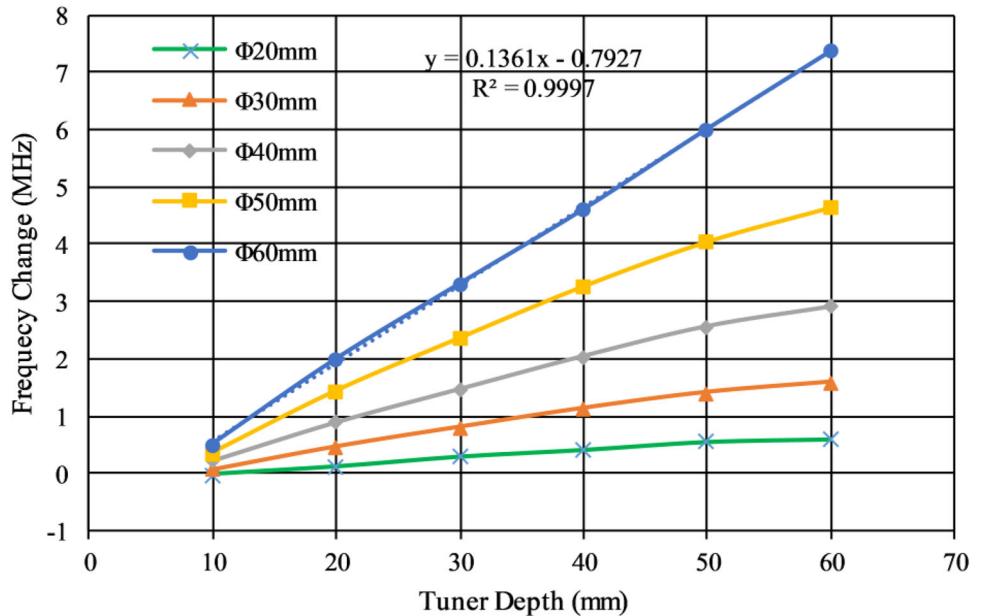


Fig. 15 (Color online) Relation between the frequency change and the tuner depth with different tuner diameters. The green (cross), orange (triangle up), gray (diamond), yellow (square), and blue (circle) curves represent tuner diameters of 20 mm, 30 mm, 40 mm, 50 mm, and 60 mm, respectively. R^2 is the trend line reliability



the pulse peak beam current in mA, and U_b is the energy gain in MV. Using typical values of 8 mA and 4 MV for I_b and U_b , respectively, we obtain a $P_b = 8 \text{ mA} \times 4 \text{ MV} = 32 \text{ kW}$. Then, the coupling factor β is given as $\beta = (P_b + P_c)/P_c = (32 \text{ kW} + 195 \text{ kW})/195 \text{ kW} = 1.16$. However, in practice, β is designed to be 1.5 for a safe margin

and is adjusted to 1.16, by rotating the angle of the coupler loop in cold testing or operation.

The longitudinal position of the coupler is at the midway point of the cavity (See Fig. 14). To avoid the ridges in the vertical plane and tuners in the horizontal plane, it is reasonable to put the coupler in a 45-degree plane (Fig. 10a). Compared with the half cavity area on the radial plane, the

coupler loop area is rather small, and hence, the magnetic field is uniform in the area where the coupler loop is located. Therefore, the coupling factor is not influenced by the shape of coupler loop, but rather, only by the size of the loop area. For ease of modeling in the RF simulation, a U-shaped loop with a radius of 2 mm was adopted to design the coupler as shown in Fig. 16a. Figure 16b plots the relation between the coupling factor β and the coupler loop area size. Figure 16c and d presents the results of the scattering parameter, and the impedance chart by the CST[®] Frequency Domain Solver with a loop area size of 3.5 cm², wherein the resonant frequency is tuned on 325 MHz and is over-coupled with a coupling coefficient of 1.5.

3.5 Summary

Based on the above design iterations, simulations, and analyses, a compact 325 MHz 7 MeV APF IH-DTL with tuners and RF power coupler (presented in Fig. 14) was designed successfully. The gap-voltage distribution was reproduced well from the beam dynamics and met all the requirements by tracking the beam dynamics with the 3D EM field exported from CST[®] MWS. A key feature of the designed DTL cavity is that its radius varies segment-wise from 95.6 to 116 mm and makes it more compact than the conventional Alvarez-type DTL. The RF operating field power of this APF IH-DTL is about 195 kW and corresponds to a quality factor of 8900. The details of the main RF characteristic parameters of the APF IH-DTL cavity were calculated by the post-processing modules of CST[®] MWS and are summarized in Table 1.

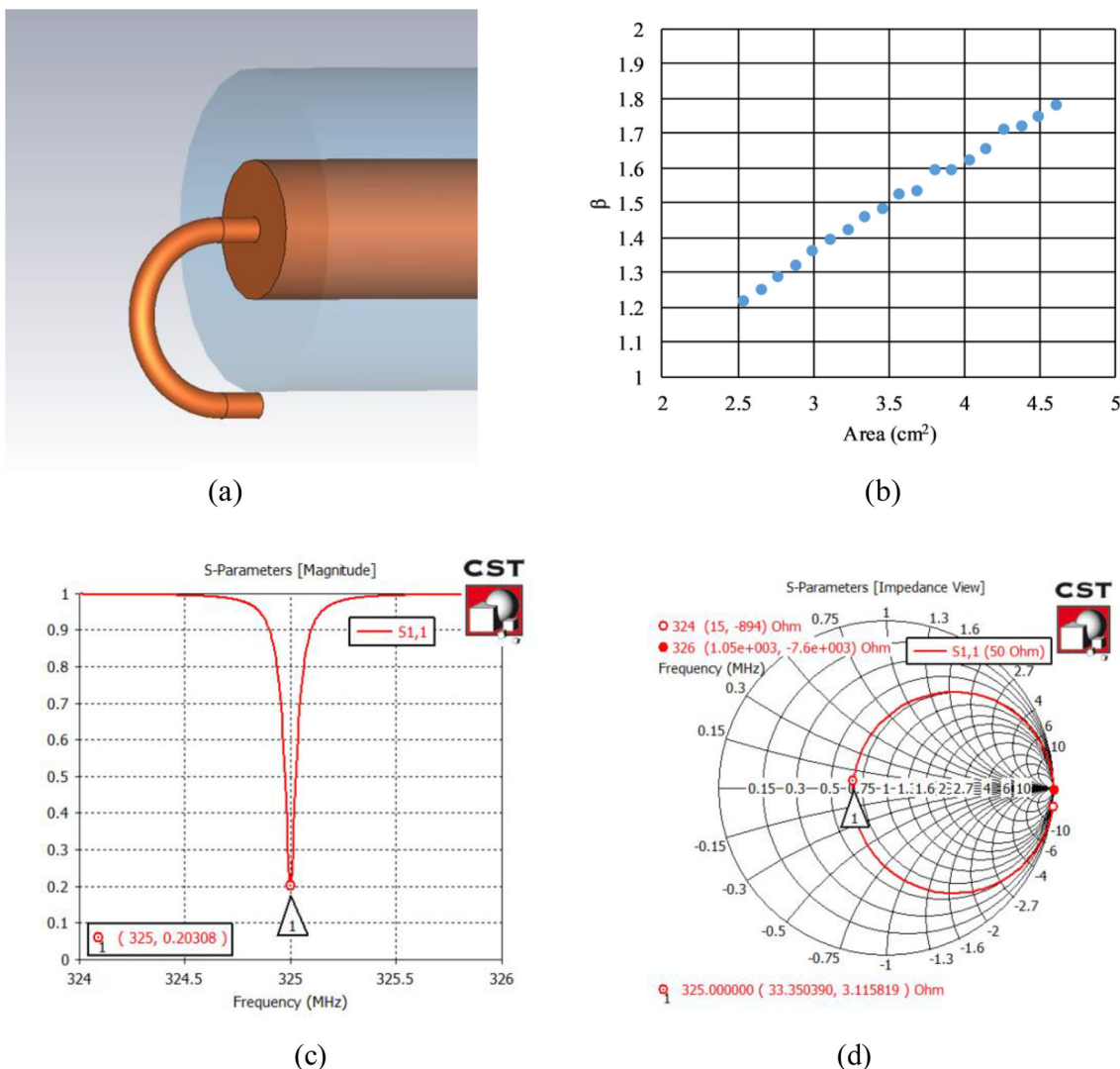


Fig. 16 (Color online) Coupler design considerations. **a** Shape of coupler, **b** relation between the coupling factor and the area of the coupler loop, **c** scattering parameter, **d** impedance chart

Table 1 Major parameters of the APF IH-DTL cavity

Parameter	Value
Operating frequency (MHz)	325
Total cavity length (mm)	1514.6
Input energy (MeV)	3
Output energy (MeV)	7
Number of unit cells	32
Inner radius of the cavity (mm)	95.6–116
Radius of the drift tube (mm)	13
Bore of the drift tube (mm)	6
Bravery factor of the cavity	1.53
Quality factor (0.8)	8900
Design operating power (0.8 <i>Q</i>) (kW)	195
Effective shunt impedance (M Ω /m)	96.6
Pulse length (μ s)	50–100
Repetition rate (Hz)	1
Duty factor (%)	0.005–0.01
Coupling factor of the coupler	1.16
Working mode	TE ₁₁₍₀₎
Number of tuners	8
Radius of tuners (mm)	30
Final normalized RMS <i>X</i> emittance (μ rad)	0.3753
Final normalized RMS <i>Y</i> emittance (μ rad)	0.3769
Synchrotron normalized RMS <i>X</i> acceptance (μ rad)	7.3428
Synchrotron normalized RMS <i>Y</i> acceptance (μ rad)	2.4476
Final momentum spread (2RMS)	$\pm 0.35\%$
Synchrotron momentum spread acceptance (2RMS)	$\pm 0.5\%$
Output pulse beam current (mA)	7
Pulse beam current requirement from synchrotron (mA)	≥ 5

4 Conclusion

The RF design and study of a compact 325 MHz 7 MeV APF IH-DTL for an injector of a proton medical accelerator was described. Through this work, an efficient APF IH-DTL RF design and optimization procedure was developed. Some main relations between the RF characteristic parameters and the structural parameters were studied and presented. Compared with the Alvarez-type DTL, the newly developed APF IH-DTL has a compact size, both radially and longitudinally. Furthermore, it uses the APF method, due to which, the cavity does not require any additional focusing elements. These features make the APF IH-DTL cost-effective and a potential candidate for the injector in the proton medical accelerator. With the machine design being completed, the cavity is currently under construction in Shanghai.

Acknowledgements We would like to express our thanks to Dr. Duan Gu for proof reading this manuscript.

References

1. F. Bray, J. Ferlay, I. Soerjomataram et al., Global cancer statistics 2018: GLOBOCAN estimates of incidence and mortality worldwide for 36 cancers in 185 countries. *Ca-Cancer J. Clin.* **68**, 394–424 (2018). <https://doi.org/10.3322/caac.21492>
2. X.C. Xie, Y.H. Pu, F. Yang et al., Design of a 7-MeV APF DTL with robust considerations. *Nucl. Instrum. Methods A.* **908**, 49–59 (2018). <https://doi.org/10.1016/j.nima.2018.08.028>
3. C.H. Miao, M. Liu, C.X. Yin et al., Precise magnetic field control of the scanning magnets for the APTRON beam delivery system. *Nucl. Sci. Tech.* **28**, 127 (2017). <https://doi.org/10.1007/s41365-017-0324-6>
4. Y.H. Yang, M.Z. Zhang, D.M. Li, Simulation study of slow extraction for the Shanghai advanced proton therapy facility. *Nucl. Sci. Tech.* **28**, 120 (2017). <https://doi.org/10.1007/s41365-017-0273-0>
5. P.F. Ma, S.X. Zheng, X.D. Yu et al., Physical design of a single-amplifier-driven proton linac injector for a synchrotron-based proton-therapy system in China. *Nucl. Instrum. Meth. A.* **900**, 32–39 (2018). <https://doi.org/10.1016/j.nima.2018.05.047>
6. G.R. Li, S.X. Zheng, H.J. Zeng et al., Design and test of an RF acceleration system loaded with magnetic alloy for the proton synchrotron of the Xi'an Proton Application Facility. *Nucl. Sci. Tech.* **29**, 94 (2018). <https://doi.org/10.1007/s41365-018-0434-9>

7. K.D. Wang, Y.J. Yuan, X.J. Yin et al., Fast-bunching design of compact heavy ion RFQ linac. *Nucl. Sci. Tech.* **29**, 180 (2018). <https://doi.org/10.1007/s41365-018-0514-x>
8. H. Shi, H.F. Ouyang, S.C. Wang et al., RF tuning and beam commissioning of CW RFQ for China-ADS Injector-I. *Nucl. Sci. Tech.* **29**, 142 (2018). <https://doi.org/10.1007/s41365-018-0478-x>
9. J.P. Blewett, in *Proceedings of the Symposium in High-Energy Accelerators and Pion Physics*. CERN, Geneva, Switzerland, 1956, p. 162
10. U. Ratzinger, *H-Type Linac Structures*. CERN Accelerator School, Lufthansa Training center, Germany, 8th-16th May 2000
11. Z.S. Li, X.J. Yin, H. Du et al., The IH-RFQ for HIRFL-CSR injector. *Nucl. Sci. Tech.* **29**, 89 (2018). <https://doi.org/10.1007/s41365-018-0416-y>
12. H. Du, Y.J. Yuan, Z.S. Li et al., Beam dynamics, RF measurement, and commissioning of a CW heavy ion IH-DTL. *Nucl. Sci. Tech.* **29**, 42 (2018). <https://doi.org/10.1007/s41365-018-0373-5>
13. T.P. Wangler, *RF Linear Accelerators*, 2nd edn. (Wiley-VCH, Weinheim, 2008)
14. Y. Iwata, S. Yamada, T. Murakami et al., Alternating-phase-focused IH-DTL for an injector of heavy-ion medical accelerators. *Nucl. Instrum. Meth. A.* **569**, 685–696 (2006). <https://doi.org/10.1016/j.nima.2006.09.057>
15. CST Studio Suite, Computer Simulation Technology (CST), <https://www.cst.com/products/csts2>. Accessed 28 Jan 2019
16. M. Otani, T. Mibe, M. Yoshida et al., Interdigital H-mode drift-tube linac design with alternative phase focusing for muon linac. *Phys. Rev. Accel. Beams.* **19**, 040101 (2016). <https://doi.org/10.1103/PhysRevAccelBeams.19.040101>
17. K. Yamamoto, H. Tanaka, H. Harada et al., Experimental verification of an APF linac for a proton therapy facility. *Nucl. Instrum. Meth. B.* **269**, 2875–2878 (2011). <https://doi.org/10.1016/j.nimb.2011.04.046>
18. W.D. Kilpatrick, Criterion for Vacuum Sparking Designed to Include Both rf and dc. *Rev. Sci. Instr.* **28**, 824 (1957). <https://doi.org/10.1063/1.1715731>
19. T.J. Boyd Jr., Kilpatrick's Criterion, Los Alamos Group AT-1 Report No. AT-1:82-28. February 12, 1982
20. Y. Iwata, T. Fujimoto, N. Miyahara et al., Model cavity of an alternating-phase-focused IH-DTL. *Nucl. Instrum. Methods A.* **566**, 256–263 (2006). <https://doi.org/10.1016/j.nima.2006.07.029>